Supplement of Atmos. Chem. Phys., 24, 3673–3698, 2024
https://doi.org/10.5194/acp-24-3673-2024-supplement

Atmospheric Chemistry and Physics
Open Access
EGU

Supplement of

Assessment of smoke plume height products derived from multisource satellite observations using lidar-derived height metrics for wildfires in the western US

Jingting Huang et al.

Correspondence to: Jingting Huang (jingting.huang@uga.edu)

Table S1: Statistical evaluation of satellite-derived wildfire SPH products against WCL-determined SPH observations using the spatial averaging method. N – the number of collocated pairs; SD – standard deviation; Q25 – lower quartile, 25% of the data lie below this value; Q50 – median, 50% of the data lie below this value; Q75 – upper quartile, 25% of the data lie above this value; MB – mean bias; MAE – mean absolute error; RMSE – root mean square error; R^2 – coefficient of determination; r – Pearson correlation coefficient.

		WCL-Determined SPH	
		SPH_{top}	SPH_{ext}
MODIS-Terra/MAIAC	N	163	
	Lidar Observations Mean ± 1 SD (km)	2.162 ± 0.542	1.382 ± 0.368
	Satellite Retrievals Mean ± 1 SD (km)	0.733 ± 0.447	
	Lidar Observations $^{Max}/_{Min}$ (km)	$^{3.903}/_{1.254}$	$^{2.253}/_{0.800}$
	Satellite Retrievals $^{Max}/_{Min}$ (km)	$^{2.114}/_{0.015}$	
	Lidar Observations Q25, Q50, Q75 (km)	1.776, 2.064, 2.508	1.131, 1.298, 1.581
	Satellite Retrievals Q25, Q50, Q75 (km)	0.438, 0.687, 0.903	
	MB (km)	-1.429	-0. 650
	MAE (km)	1.429	0.673
	RMSE (km)	1.591	0.822
	R^2	-7.618	-3.995
	r	0.008	**0.247** **
MODIS-Aqua/MAIAC	N	114	
	Lidar Observations Mean ± 1 SD (km)	2.686 ± 0.797	1.790 ± 0.644
	Satellite Retrievals Mean ± 1 SD (km)	0.425 ± 0.262	
	Lidar Observations $^{Max}/_{Min}$ (km)	$^{4.215}/_{1.374}$	$^{3.422}/_{0.800}$
	Satellite Retrievals $^{Max}/_{Min}$ (km)	$^{0.935}/_{0.025}$	
	Lidar Observations Q25, Q50, Q75 (km)	2.063, 2.627, 3.350	1.274, 1.728, 2.325
	Satellite Retrievals Q25, Q50, Q75 (km)	0.192, 0.379, 0.697	
	MB (km)	-2.261	-1.365
	MAE (km)	2.261	1.365
	RMSE (km)	2.393	1.525
	R^2	-8.009	-4.617
	r	**0.219** *	0.057
MISR/MERLIN	N	90	
	Lidar Observations Mean ± 1 SD (km)	2.216 ± 0.506	1.498 ± 0.449
	Satellite Retrievals Mean ± 1 SD (km)	2.124 ± 0.625	
	Lidar Observations $^{Max}/_{Min}$ (km)	$^{2.982}/_{1.254}$	$^{2.253}/_{0.853}$
	Satellite Retrievals $^{Max}/_{Min}$ (km)	$^{3.029}/_{0.625}$	
	Lidar Observations Q25, Q50, Q75 (km)	1.791, 2.204, 2.648	1.129, 1.428, 1.969
	Satellite Retrievals Q25, Q50, Q75 (km)	1.658, 2.083, 2.801	
	MB (km)	-0.092	0. 626
	MAE (km)	0.368	0.719
	RMSE (km)	0.554	0.788
	R^2	-0.196	-2.076
	r	**0.551** **	**0.648** **

Table S1: Cont.

		WCL-Determined SPH	
		SPH_{top}	**SPH_{ext}**
VIIRS/ASHE	N	130	
	Lidar Observations Mean ± 1 SD (km)	2.823 ± 0.999	1.895 ± 0.890
	Satellite Retrievals Mean ± 1 SD (km)	2.707 ± 1.149	
	Lidar Observations $^{Max}/_{Min}$ (km)	$^{5.493}/_{1.497}$	$^{4.003}/_{0.811}$
	Satellite Retrievals $^{Max}/_{Min}$ (km)	$^{4.603}/_{0.227}$	
	Lidar Observations Q25, Q50, Q75 (km)	1.977, 2.904, 3.318	1.094, 1.629, 2.489
	Satellite Retrievals Q25, Q50, Q75 (km)	2.263, 2.661, 3.625	
	MB (km)	-0.106	0.823
	MAE (km)	1.196	1.599
	RMSE (km)	1.694	1.814
	R^2	-1.876	-3.152
	r	**-0.236** *	**-0.246** *
TROPOMI/ALH	N	127	
	Lidar Observations Mean ± 1 SD (km)	2.677 ± 1.075	1.894 ± 0.936
	Satellite Retrievals Mean ± 1 SD (km)	2.001 ± 0.541	
	Lidar Observations $^{Max}/_{Min}$ (km)	$^{5.493}/_{1.374}$	$^{4.003}/_{0.734}$
	Satellite Retrievals $^{Max}/_{Min}$ (km)	$^{3.425}/_{1.412}$	
	Lidar Observations Q25, Q50, Q75 (km)	1.718, 2.337, 3.308	1.019, 1.542, 2.684
	Satellite Retrievals Q25, Q50, Q75 (km)	1.546, 1.759, 2.391	
	MB (km)	-0.676	0.107
	MAE (km)	0.850	0.843
	RMSE (km)	1.324	0.980
	R^2	-0.518	-0.094
	r	0.130	**0.218** *

*Note that r in bold demonstrate a statistically significant relationship between the two variables; the symbol * signifies a p value < 0.05 and ** indicates a p value < 0.01. A lower p-value suggests a higher level of statistical significance.*

Table S2: Statistical evaluation of satellite-derived wildfire SPH products against WCL-determined SPH observations using the matched-pair method. N – the number of collocated pairs; SD – standard deviation; Q25 – lower quartile, 25% of the data lie below this value; Q50 – median, 50% of the data lie below this value; Q75 – upper quartile, 25% of the data lie above this value; MB – mean bias; MAE – mean absolute error; RMSE – root mean square error; R^2 – coefficient of determination; r – Pearson correlation coefficient.

		WCL-Determined SPH	
		SPH_{top}	SPH_{ext}
MODIS-Terra/MAIAC	N	163	
	Lidar Observations Mean ± 1 SD (km)	2.162 ± 0.542	1.382 ± 0.368
	Satellite Retrievals Mean ± 1 SD (km)	0.700 ± 0.550	
	Lidar Observations $^{Max}/_{Min}$ (km)	$^{3.903}/_{1.254}$	$^{2.253}/_{0.800}$
	Satellite Retrievals $^{Max}/_{Min}$ (km)	$^{2.650}/_{0.004}$	
	Lidar Observations Q25, Q50, Q75 (km)	1.776, 2.064, 2.508	1.131, 1.298, 1.581
	Satellite Retrievals Q25, Q50, Q75 (km)	0.325, 0.643, 0.952	
	MB (km)	-1.462	-0. 683
	MAE (km)	1.462	0.737
	RMSE (km)	1.664	0.919
	R^2	-8.419	-5.246
	r	-0.055	0.146
MODIS-Aqua/MAIAC	N	114	
	Lidar Observations Mean ± 1 SD (km)	2.686 ± 0.797	1.790 ± 0.644
	Satellite Retrievals Mean ± 1 SD (km)	0.370 ± 0.258	
	Lidar Observations $^{Max}/_{Min}$ (km)	$^{4.215}/_{1.374}$	$^{3.422}/_{0.800}$
	Satellite Retrievals $^{Max}/_{Min}$ (km)	$^{1.109}/_{0.025}$	
	Lidar Observations Q25, Q50, Q75 (km)	2.063, 2.627, 3.350	1.274, 1.728, 2.325
	Satellite Retrievals Q25, Q50, Q75 (km)	0.146, 0.308, 0.579	
	MB (km)	-2.317	-1.419
	MAE (km)	2.315	1.419
	RMSE (km)	2.444	1.564
	R^2	-8.398	-4.904
	r	**0.220** *	0.148
MISR/MERLIN	N	90	
	Lidar Observations Mean ± 1 SD (km)	2.216 ± 0.506	1.498 ± 0.449
	Satellite Retrievals Mean ± 1 SD (km)	2.114 ± 0.731	
	Lidar Observations $^{Max}/_{Min}$ (km)	$^{2.982}/_{1.254}$	$^{2.253}/_{0.853}$
	Satellite Retrievals $^{Max}/_{Min}$ (km)	$^{3.480}/_{0.625}$	
	Lidar Observations Q25, Q50, Q75 (km)	1.791, 2.204, 2.648	1.129, 1.428, 1.969
	Satellite Retrievals Q25, Q50, Q75 (km)	1.576, 1.965, 2.729	
	MB (km)	-0.102	0. 616
	MAE (km)	0.494	0.782
	RMSE (km)	0.688	0.867
	R^2	-0.846	-2.726
	r	**0.444** **	**0.556** **

Table S2: Cont.

		WCL-Determined SPH	
		SPH_{top}	**SPH_{ext}**
VIIRS/ASHE	N	130	
	Lidar Observations Mean ± 1 SD (km)	2.823 ± 0.999	1.895 ± 0.890
	Satellite Retrievals Mean ± 1 SD (km)	2.707 ± 1.165	
	Lidar Observations $^{Max}/_{Min}$ (km)	$^{5.493}/_{1.497}$	$^{4.003}/_{0.811}$
	Satellite Retrievals $^{Max}/_{Min}$ (km)	$^{4.930}/_{0.231}$	
	Lidar Observations Q25, Q50, Q75 (km)	1.977, 2.904, 3.318	1.094, 1.629, 2.489
	Satellite Retrievals Q25, Q50, Q75 (km)	2.060, 2.683, 3.579	
	MB (km)	-0.116	0.812
	MAE (km)	1.190	1.594
	RMSE (km)	1.697	1.806
	R^2	-1.887	-3.115
	r	**-0.220** *	**-0.220** *
TROPOMI/ALH	N	127	
	Lidar Observations Mean ± 1 SD (km)	2.677 ± 1.075	1.894 ± 0.936
	Satellite Retrievals Mean ± 1 SD (km)	2.052 ± 0.588	
	Lidar Observations $^{Max}/_{Min}$ (km)	$^{5.493}/_{1.374}$	$^{4.003}/_{0.734}$
	Satellite Retrievals $^{Max}/_{Min}$ (km)	$^{3.425}/_{1.412}$	
	Lidar Observations Q25, Q50, Q75 (km)	1.718, 2.337, 3.308	1.019, 1.542, 2.684
	Satellite Retrievals Q25, Q50, Q75 (km)	1.546, 1.802, 2.431	
	MB (km)	-0.625	0.158
	MAE (km)	0.832	0.847
	RMSE (km)	1.304	0.991
	R^2	-0.472	-0.121
	r	0.151	**0.241** **

*Note that r in bold demonstrate a statistically significant relationship between the two variables; the symbol * signifies a p value < 0.05 and ** indicates a p value < 0.01. A lower p-value suggests a higher level of statistical significance.*

Table S3: Location and elevation above mean sea level (AMSL) of balloon sounding stations near the UWKA flight operations during the August 2018 BB-FLUX project.

Station ID	Latitude	Longitude	Elevation (m AMSL)
BOI	43.56	-116.21	874
LKN	40.86	-115.73	1608
MFR	42.36	-122.86	405
SLC	40.77	-111.95	1289

Table S4: Physical schemes used in the WRF simulations. A 4 km (grid spacing) domain across the western US with a domain size of 629 × 501 (east-west direction × north-south direction) in the WRF configuration is centered at 40° N and 116° W.

Physical Process	Scheme
Microphysics	Purdue Lin Scheme (Chen and Sun, 2002)
Convection	Grell–Devenyi Ensemble Scheme (Grell and Dévényi, 2002)
Short/Long-wave radiation	RRTMG Shortwave and Longwave Schemes (Iacono et al., 2008)
Planetary boundary layer	Yonsei University scheme (Hong et al., 2006)
Surface layer	Revised MM5 Scheme (Jiménez et al., 2012)
Land surface	Unified Noah Land Surface Model (Tewari et al., 2004)

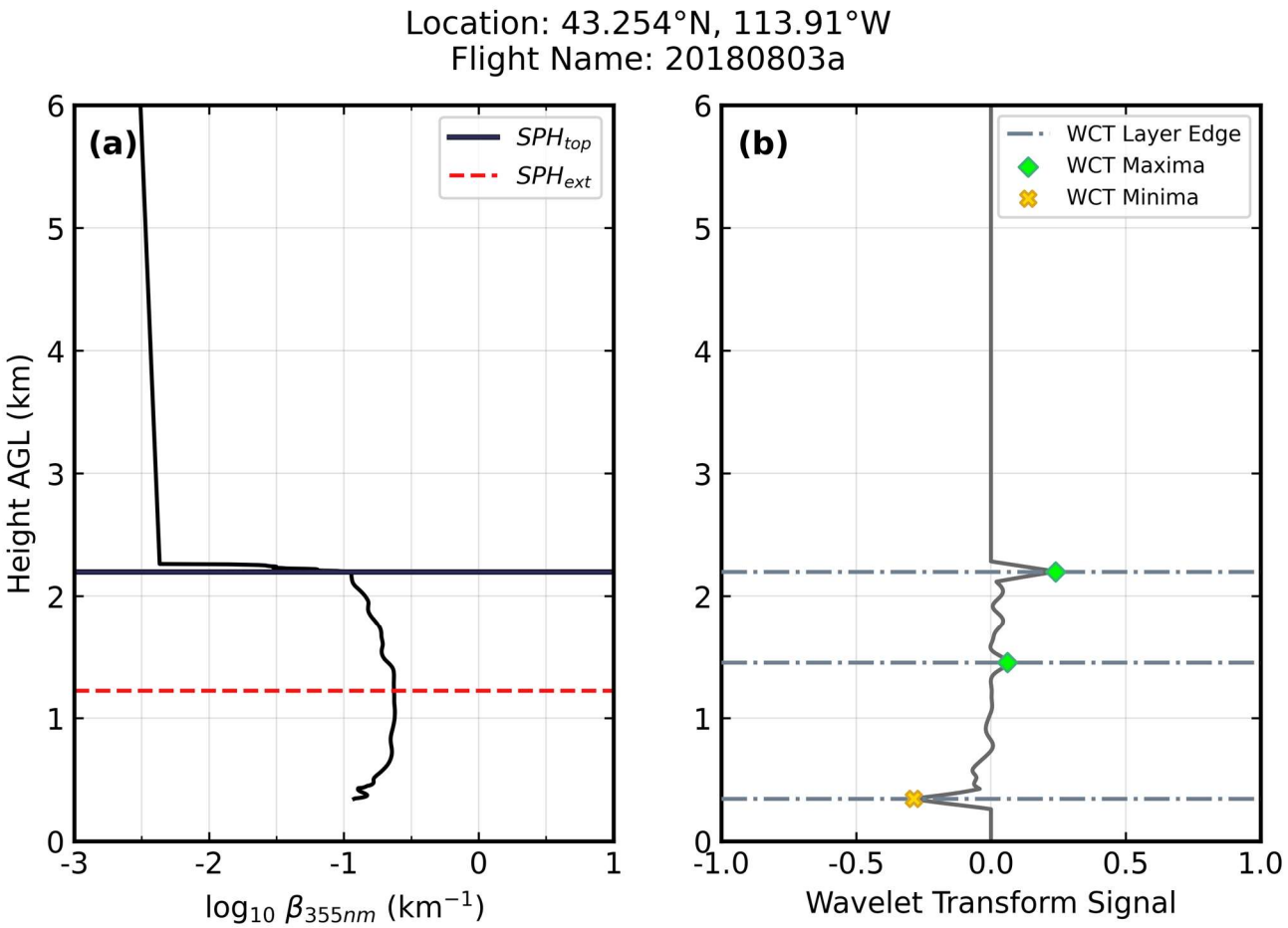

Figure S1: An example of a single-layered aerosol structure is presented here, as evidenced by (a) the WCL aerosol extinction coefficient profile at 355 nm derived from the composite airborne lidar vertical cross-section, and (b) the resulting WCT profile, on August 3, 2018, at a location (43.254° N, 113.91° W). In panel (a), the dashed red line represents the calculated SPH_{top}, while the calculated SPH_{ext} is shown as the solid blue line for comparison. In panel (b), the WCT-detected aerosol layer top (or bottom) is marked by the horizontal dash-dotted grey line. Chromatic icons denote the local maxima (green, "diamond") and minima (yellow, "x") of the signal obtained by the WCT methodology.

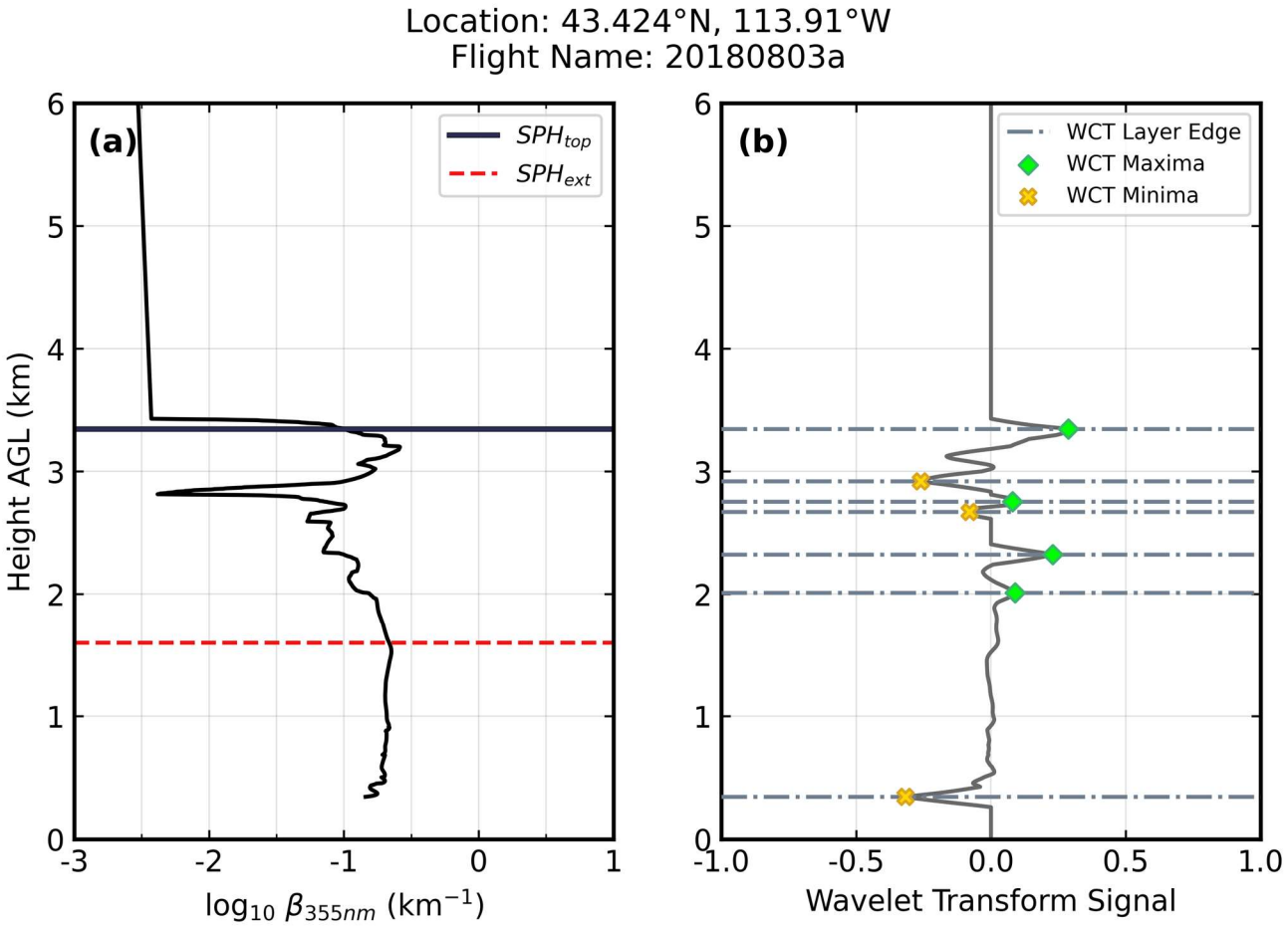

Figure S2: Another example has the same logic as shown in Figure S1, but for a multi-layered aerosol structure case on August 3, 2018, at a location (43.424° N, 113.91° W).

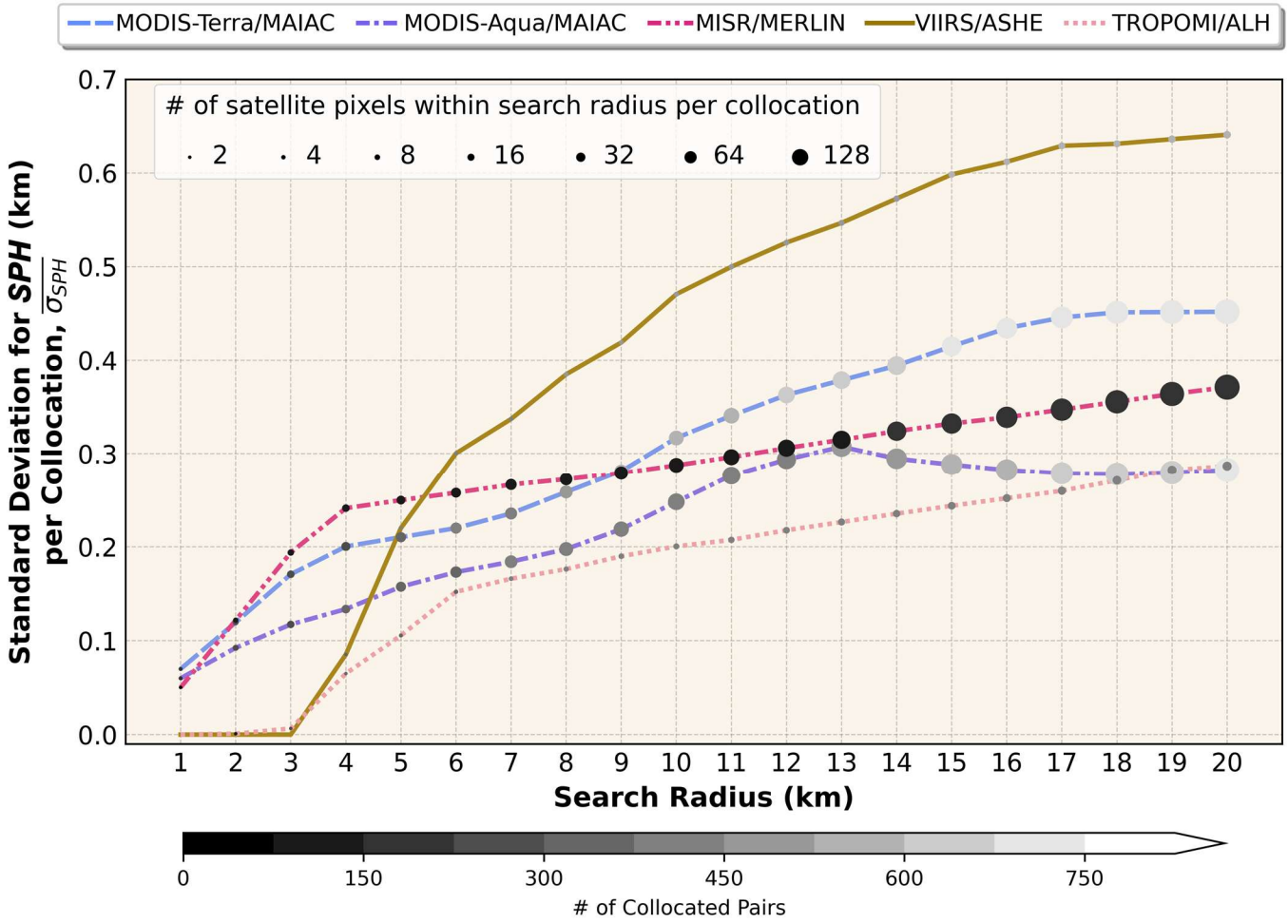

Figure S3: The SD for SPH per collocation across various satellite products (MODIS-Terra/MAIAC, MODIS-Aqua/MAIAC, MISR/MERLIN, VIIRS/ASHE, and TROPOMI/ALH) as a function of the search radius, which pertains to all successful collocations during the August 2018 BB-FLUX field campaign, with a 12-minute searching time window. The color bar indicates the total number of collocated pairs between satellite retrievals and lidar observations. The larger the scatter point size, the greater the number of satellite pixels within the circular area defined by a given search radius. A workflow for the collocation methodology is outlined as follows. First, satellite pixels within a 1 km to 20 km distance from a given lidar point, and whose observation time falls within 12 minutes of that point, are only selected. From this subset, a nearest-neighbor search identifies the closest satellite pixel to the lidar point. When that collocation is found, any nearby satellite pixels within the circular area of a specific search radius are also counted. The collocation process extracts and records data such as the satellite-retrieved SPH value, lidar-determined SPH value, collocation's geolocations, and the number of satellite pixels in the sampling area around the lidar point. Second, as shown in Figure S3, the search radius range is narrowed down when the SDs of the satellite-retrieved SPH products are above zero and when there are at least two adjacent satellite pixels. Finally, the optimal search radius is determined based on the total number of collocations, while ensuring minimal variation in the satellite-retrieved SPH values.

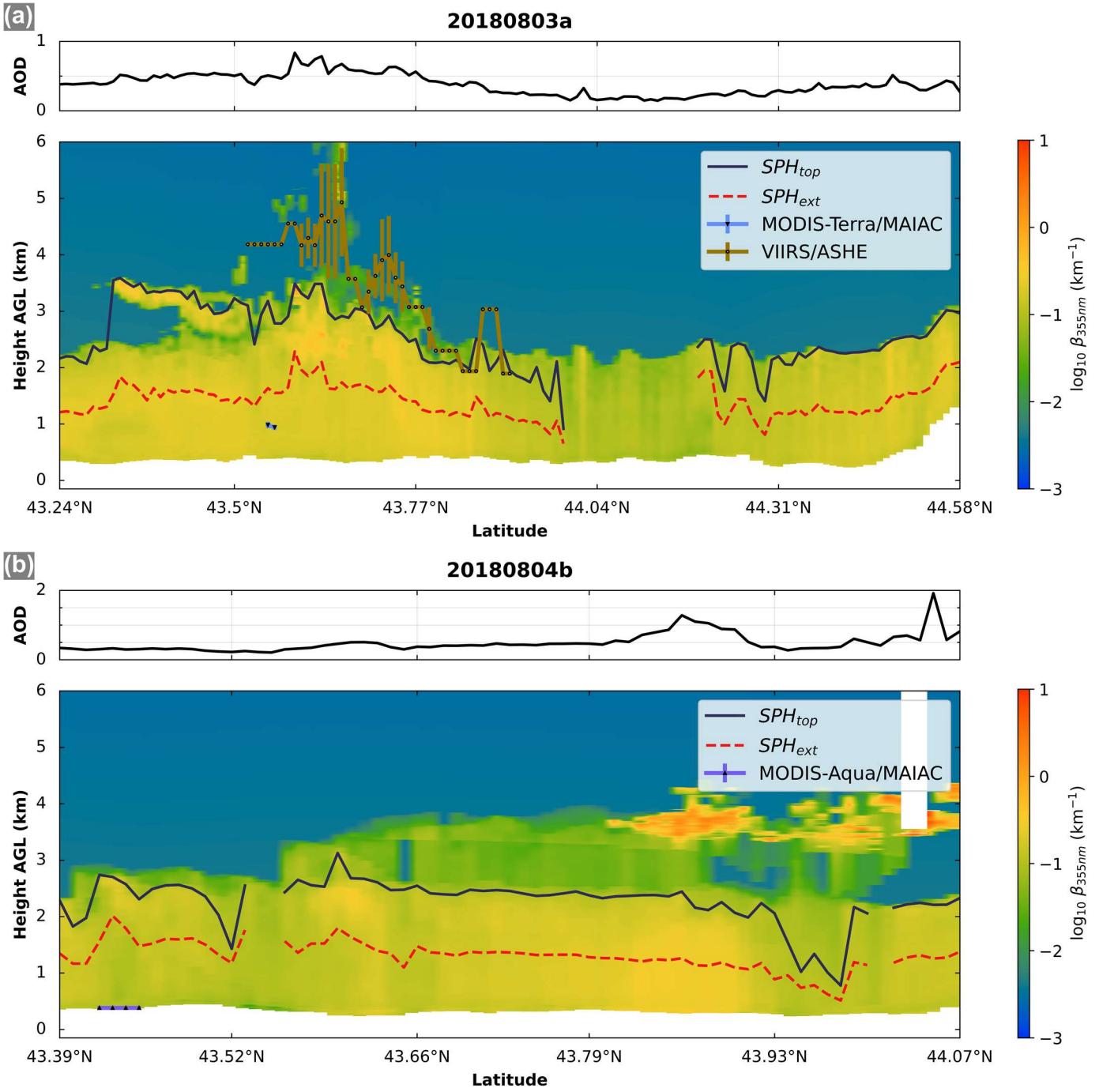

Figure S4: Composite latitude–height cross-sections of WCL vertical aerosol extinction coefficient at 355 nm covering other nine reconstructed flight tracks from the August 2018 BB-FLUX campaign: (a) 0803a; (b) 0804b; (c) 0808b; (d) 0812a; (e) 0820a; (f) 0820b; (g) 0823a; (h) 0824a; (i) 0825a. These cross-sections are overlaid with WCL-determined SPHs (i.e., SPH_{top} and SPH_{ext}) and satellite-retrieved SPHs, along with corresponding AOD variations.

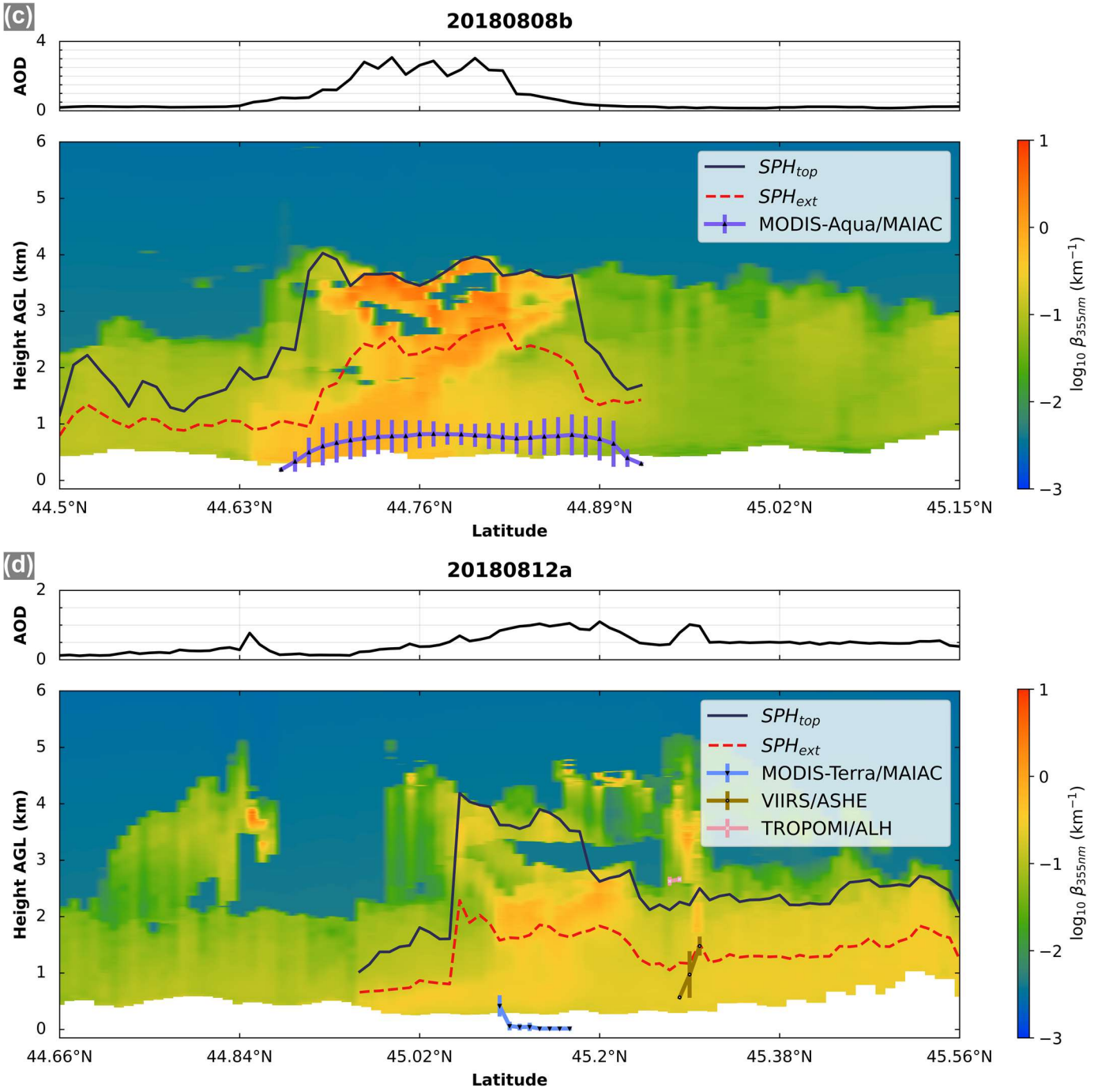

Figure S4: Cont.

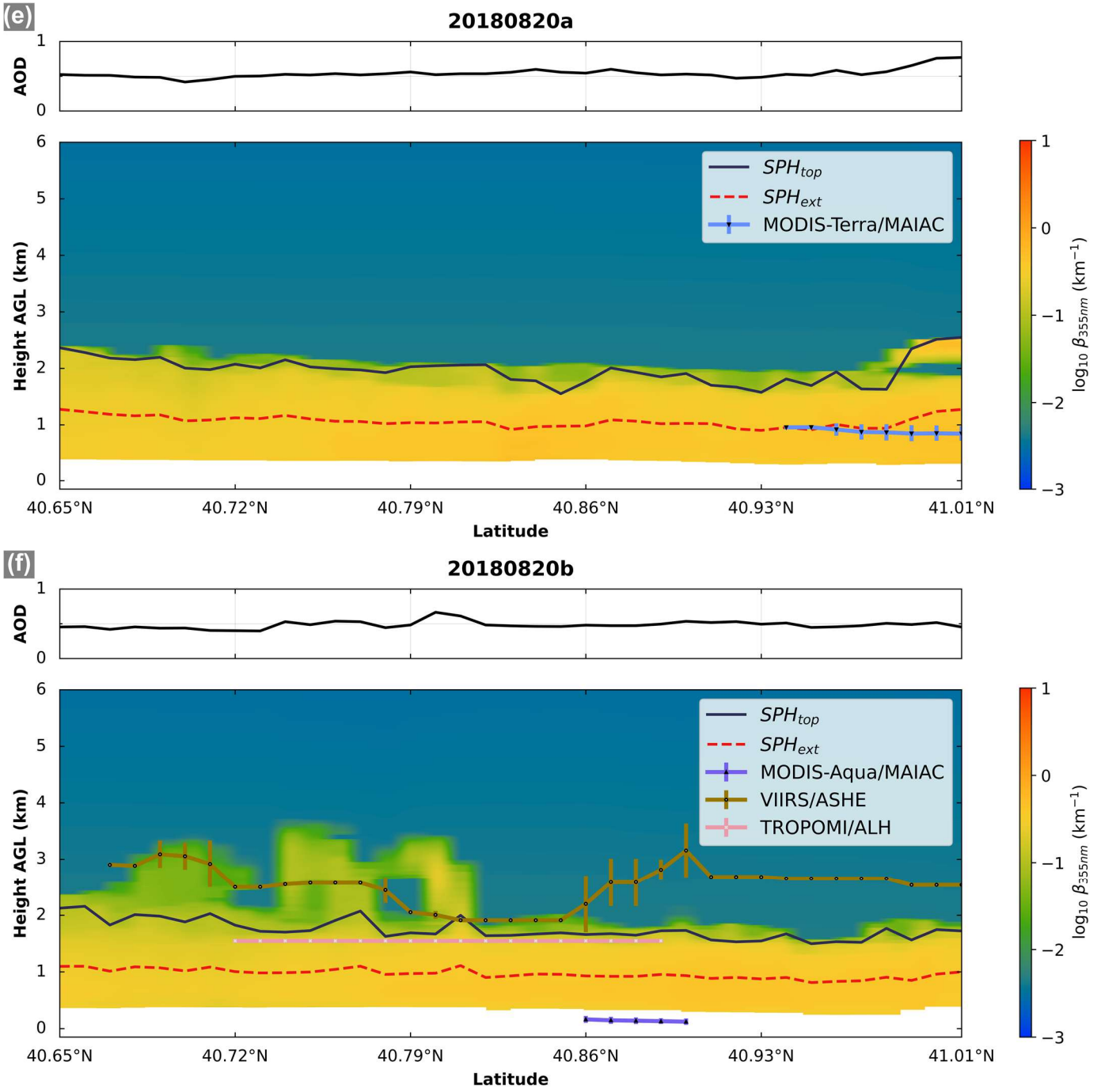

Figure S4: Cont.

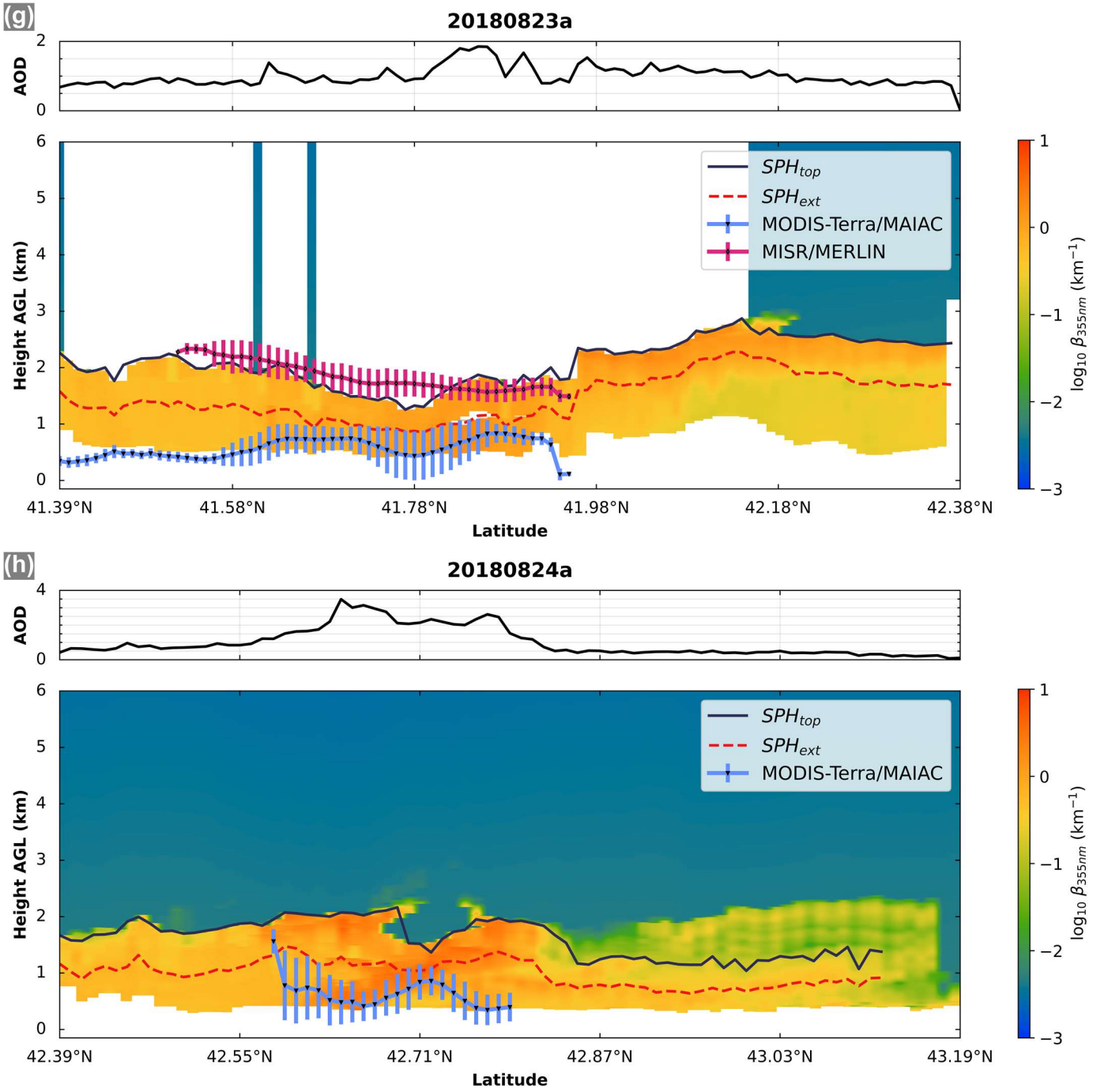

Figure S4: Cont.

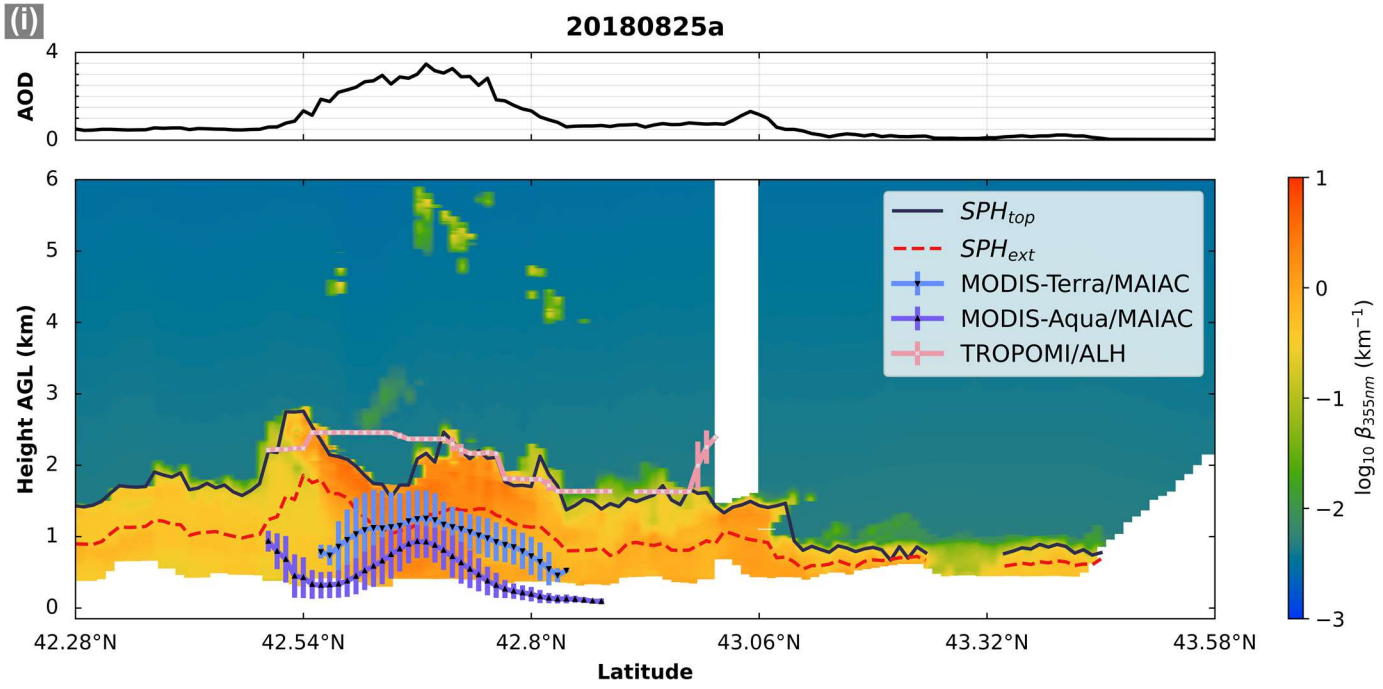

Figure S4: Cont.

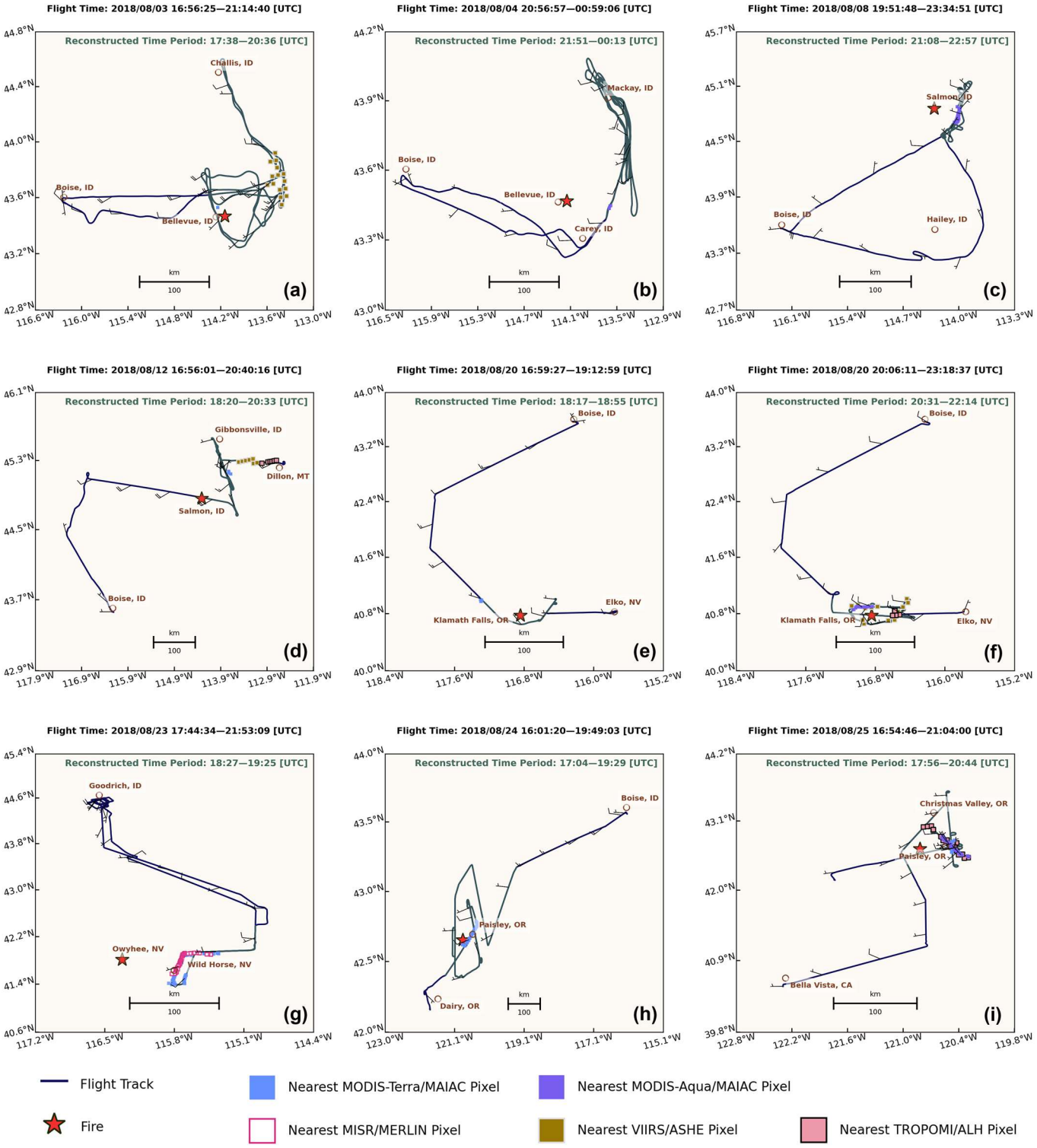

Figure S5: The other nine UWKA flight tracks selected from the August 2018 BB-FLUX campaign. These tracks are highlighted by their reconstructed time periods and associated with five different types of satellite collocations: (a) 0803a; (b) 0804b; (c) 0808b; (d) 0812a; (e) 0820a; (f) 0820b; (g) 0823a; (h) 0824a; (i) 0825a.

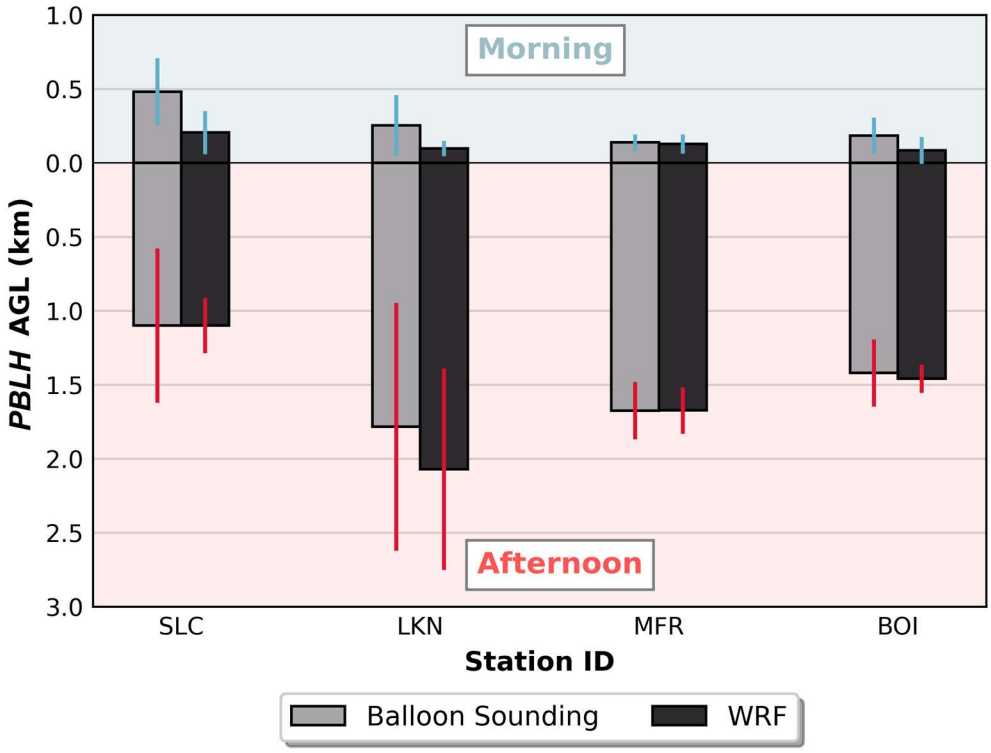

Figure S6: PBLH averages (with error bars) at 00Z (Afternoon) and at 12Z (Morning), from balloon soundings and WRF simulations in August 2018. Due to uncertainties in the PBLH values computed by the WRF model, these are not used directly. Instead, hourly WRF PBLH is re-calculated in the same way as the balloon data, using either the vertical potential temperature gradient method or the Richardson number method.

References

Chen, S.-H. and Sun, W.-Y.: A one-dimensional time dependent cloud model, J. Meteorol. Soc. of Jpn. Ser. II, 80, 99–118, https://doi.org/10.2151/jmsj.80.99, 2002.

Grell, G. A. and Dévényi, D.: A generalized approach to parameterizing convection combining ensemble and data assimilation techniques, Geophys. Res. Lett., 29, 1693, https://doi.org/10.1029/2002GL015311, 2002.

Hong, S.-Y., Noh, Y., and Dudhia, J.: A new vertical diffusion package with an explicit treatment of entrainment processes, Mon. Weather Rev., 134, 2318–2341, https://doi.org/10.1175/MWR3199.1, 2006.

Iacono, M. J., Delamere, J. S., Mlawer, E. J., Shephard, M. W., Clough, S. A., and Collins, W. D.: Radiative forcing by long-lived greenhouse gases: Calculations with the AER radiative transfer models, J. Geophys. Res.-Atmos., 113, D13103, https://doi.org/10.1029/2008JD009944, 2008.

Jiménez, P. A., Dudhia, J., González-Rouco, J. F., Navarro, J., Montávez, J. P., and García-Bustamante, E.: A revised scheme for the WRF surface layer formulation, Mon. Weather Rev., 140, 898–918, https://doi.org/10.1175/MWR-D-11-00056.1, 2012.

Tewari, M., Chen, F., Wang, W., Dudhia, J., LeMone, M. A., Mitchell, K., Ek, M., Gayno, G., Wegiel, J., and Cuenca, R. H.: Implementation and verification of the unified noah land sur face model in the WRF model [presentation], in: 20th Confer ence on Weather Analysis and Forecasting/16th Conference on Numerical Weather Prediction, 11–15 January, http://n2t.net/ark:/85065/ d7fb523p (last access: 11 June 2023), 2004.